Title: CFTR potentiation by VX-770 involves stabilization of the pre-hydrolytic, O_1 state

Running Title: VX-770 mechanism involves stabilization of O_1

Emily Langron, Stella Prins and Paola Vergani

Neuroscience, Physiology and Pharmacology

University College London

Gower Street

London WC1E 6BT

Correspondence to: emily.langron.12@ucl.ac.uk; p.vergani@ucl.ac.uk

Word count (excluding Methods and References): 5310

Abstract

BACKGROUND AND PURPOSE

Cystic fibrosis (CF) is a debilitating hereditary disease caused by mutations in the *CFTR* gene, which encodes an anion channel. WT-CFTR gating is a non-equilibrium process. After ATP binding, CFTR enters a stable open state (O_1). ATP hydrolysis leads it to a short-lived post-hydrolytic open state (O_2), from which channels close. Here we use mutations to probe the mechanism of VX-770, the first compound directly targeting the CFTR protein approved for treatment of CF. D1370N and K1250R mutations greatly reduce or abolish catalytic activity, simplifying the gating scheme to an equilibrium ($C \leftrightarrow O_1$); K464A-CFTR has a destabilized O_1 state and rarely closes via hydrolysis.

EXPERIMENTAL APPROACH

Potentiation by VX-770 was measured using microscopic imaging of HEK293 cells expressing an anion-sensitive YFP-CFTR. A simple mathematical model was used to predict fluorescence quenching following extracellular iodide addition, and estimate CFTR conductance. Membrane density of CFTR channels was measured in a parallel assay, using CFTR-pHTomato.

KEY RESULTS

VX-770 strongly potentiates WT-CFTR, D1370N-CFTR and K1250R-CFTR. K464A-CFTR was also strongly potentiated, regardless of whether it retained catalytic activity or not.

CONCLUSIONS AND IMPLICATIONS

Similar potentiation of hydrolytic and non-hydrolytic mutants suggests that VX-770 increases CFTR open probability mainly by stabilising the pre-hydrolytic O_1 state with respect to the closed state. Potentiation of K464A-CFTR channels suggests action of the drug does not strongly alter conformational dynamics at site 1. Understanding potentiator mechanism could help develop improved treatment for CF patients. The fluorescence assay presented here is a robust tool for such investigations.

Abbreviations

ABC	ATP-binding cassette
CF	Cystic Fibrosis
CFTR	Cystic Fibrosis Transmembrane Conductance Regulator
ΔF_M	change in fluorescence reporting on membrane-localised CFTR-pHTomato
EC_{50}	half-maximal effective concentration
F/F_{max}	normalized YFP fluorescence
$F_{pHTomato}$	weighted average fluorescence obtained in pHTomato assay
G_{CFTR}	CFTR conductance
G_{trans}	transient anion conductance
IRES	internal ribosome entry site
MES	2-(N-morpholino)ethanesulfonic acid
NBD	nucleotide binding domain
PDL	poly-D-lysine
P_o	open probability
SSR	sum of squared residuals
τ_{trans}	time constant of the transient anion conductance
V_M	membrane potential
WT	wild type
YFP	yellow fluorescent protein

Introduction

Mutations in the cystic fibrosis transmembrane conductance regulator (*CFTR*) gene cause cystic fibrosis (CF), a common lethal hereditary disease (Riordan et al., 1989). CFTR is a member of the ATP-binding cassette (ABC) superfamily of transporters, but it is unique in its function as an ion channel, allowing passive anion flow across the plasma membrane.

Protein Kinase A (PKA)-dependent phosphorylation of the unique regulatory (R)-domain is required for sustained gating (Chang et al., 1993). Once channels are phosphorylated, ATP binding at two cytosolic nucleotide binding domains (NBDs) favours pore opening in the transmembrane domains. Opening is coupled to formation of an NBD dimer, with ATP bound at composite binding sites formed at the NBD interface (Fig. 1; Vergani et al., 2003, 2005). The channel remains open until ATP hydrolysis at catalytic site 2 (Csanády et al., 2010), triggers entry into a short-lived, post-hydrolytic O_2 state, from which closing occurs rapidly (Gunderson and Kopito, 1995). ATP at site 1 remains bound for many gating cycles (Tsai et al., 2010), although conformational changes associated with gating and linked to partial site 1 opening of the dimer interface have been demonstrated (Csanady et al., 2013; Chaves and Gadsby, 2015).

The approval of VX-770 (Ivacaftor; Vertex Pharmaceuticals) marked a step forward in treatment for CF. VX-770 was the first drug to target the CFTR channel directly, rather than disease symptoms. It is now approved to treat CF caused by a number of gating mutations (Van Goor et al., 2009, 2014; Yu et al., 2012), and the impact in the clinic has been very positive (Ramsey et al., 2011; Davies et al., 2013).

VX-770 is a potentiator, a compound which increases the open probability (P_o) of CFTR (Van Goor et al., 2009). At millimolar, physiological, ATP concentrations it causes a marked prolongation of mean open time, and a modest increase in opening rate, as seen in single channel patch-clamp experiments (Yu et al., 2012; Jih and Hwang, 2013). VX-770 increases the mean open time of both wild type (WT)-CFTR channels, which gate via the non-equilibrium mechanism outlined above (Vergani et al., 2005; Csanády et al., 2010), and G551D-CFTR channels, which gate via an equilibrium mechanism retaining little ATP sensitivity (Bompadre et al., 2007; Lin et al., 2014). It has been hypothesised that VX-770 achieves this mainly via stabilisation of the post-hydrolytic O_2 state (Jih and Hwang, 2013). However, Kopeikin et al. (2014) demonstrate that the closing rate of E1371S-CFTR, a non-hydrolytic mutant (Vergani et al., 2003), is slowed by VX-770. Slowed closure of E1371S-

CFTR channels cannot be caused by a stabilised O_2 state. To further investigate how VX-770 interacts with open CFTR channels, gating mutants, whose gating kinetics have been extensively characterised, were used to alter open state stability and thus manipulate the proportion of time spent in the O_1 and O_2 states.

WT-CFTR open bursts are initiated after ATP-binding at site 2 (lower site; Fig. 1), and terminated following hydrolysis of that ATP. The rate of non-hydrolytic closure (k_{-1}, $O_1 \rightarrow C$) is slow compared to hydrolysis (k_1, $O_1 \rightarrow O_2$), so almost no events close via the backward non-hydrolytic closing pathway (Fig. 1; Csanády et al., 2010), resulting in non-equilibrium cycling between conformations (central arrow, Fig. 1).

Mutations of catalytic residues in site 2 can block the hydrolytic pathway to closure. D1370 and K1250 are the Walker B aspartate and the Walker A lysine, respectively, in NBD2 (Walker et al., 1982). Atomic level determination of the structure of ABC transporters and CFTR (e.g. Yuan et al., 2001; Smith et al., 2002; Chen et al., 2003; Zhang et al., 2017) confirmed their role as key catalytic residues within site 2. The corresponding mutations in other ABC transporters have been shown to abolish hydrolytic activity (Urbatsch et al., 1995; Lerner-Marmarosh et al., 1999; Rai et al., 2006). In CFTR, prolonged burst durations are observed for D1370N-CFTR and K1250R-CFTR (Vergani et al., 2003, 2005; Csanády et al., 2010), D1370N-CFTR does not enter a higher conductance post-hydrolytic state discernible in specific conditions (Gunderson and Kopito, 1995), and open dwell-time distributions are consistent with virtually all opening events terminating via the non-hydrolytic closing pathway (Csanády et al., 2010). The underlying gating cycle is likely very similar for K1250R-CFTR, with both non-hydrolytic mutants never entering the post-hydrolytic O_2 state during ATP-dependent gating.

K464 is the Walker A lysine of NBD1. Despite being part of the degenerate, non-catalytic site 1, the alanine replacement in K464A-CFTR reduces the turnover rate of ATP hydrolysis ~10-fold (Ramjeesingh et al., 1999). Dwell-time distribution analysis suggests that this is due to the vast majority of K464A-CFTR opening events closing via the non-hydrolytic pathway, thus reducing the proportion of openings undergoing hydrolysis (Fig. 1; Csanády et al., 2010). This, and other experimental results (Powe Jr et al., 2002; Vergani et al., 2003; Bompadre et al., 2005), suggest that the K464A mutation destabilizes the pre-hydrolytic open state O_1, with respect to the opening transition state, decreasing the energetic barrier for backward non-hydrolytic closure. Because VX-770 slows closure of E1371S-CFTR channels

(Kopeikin et al., 2014) - which is most simply interpreted as due to a stabilization by the drug of the pre-hydrolytic open state O_1 with respect to the opening transition state - VX-770 and the K464A mutation appear to affect O_1 stability in opposite ways. To investigate whether the drug and site 1 mutation might be affecting CFTR structure and dynamics via a similar mechanism, we tested the effect of VX-770 on K464A-CFTR channels.

We used cell-based assays exploiting genetically encoded fluorescent proteins tagged to CFTR (Langron et al., 2017), to study how VX-770 alters CFTR gating. In this system the CFTR proteins are embedded in mammalian membranes and exposed to a physical and chemical environment (e.g. physiological cytosolic ionic and ATP concentrations, presence of cytoskeleton, of anchoring proteins etc.) very close to those present in the native epithelial cells. While such fluorescence assays do not have the exquisite sensitivity of electrophysiological techniques allowing detection of gating events at the single channel level, they provide a robust, informative readout of the overall functional changes drugs cause on populations of CFTR channels.

Methods

Materials and cell culture

VX-770 and VX-809 were purchased from Selleck Chemicals. All other chemicals were purchased from Sigma-Aldrich. HEK-293 cells were maintained in DMEM, supplemented with 2 mM L-glutamine, 100 U/ml penicillin and streptomycin, and 10% FBS (Life Technologies). For fluorescence imaging, cells were seeded in poly-D-lysine (PDL)-coated, black walled 96-well plates (Costar, Fisher Scientific).

Plasmids and transfections

eGFP-CFTR in pcDNA3.1 (a gift from Bruce Stanton, Geisel School of Medicine, NH), in which eGFP is tagged to the N-terminal of CFTR via a 23 amino-acid linker, was mutated to yellow fluorescent protein (YFP)-CFTR using site-directed mutagenesis (introducing F46L, L64F, S65G, V68L, S72A, H148Q, I152L and T203Y, see Langron et al., 2017; Quikchange protocol, Stratagene). pIRES2-eGFP-CFTR was a gift from David Gadsby (Rockefeller University, NY). pHTomato (provided by Dr Li, Peking University, China, and Prof. Richard Tsien, NYU School of Medicine, NY), was inserted after position 901 in CFTR, using a primer overlap-extension strategy. pIRES2-CFTR-pHTomato contained eGFP under control of an internal ribosome entry site (IRES), which allows transcription of a single mRNA containing eGFP and CFTR-pHTomato sequences, but translation of the two as separate proteins (Langron et al., 2017). Point mutations were introduced to pcDNA3.1-YFP-CFTR and pIRES2-CFTR-pHTomato using site-directed mutagenesis (Quikchange protocol, Stratagene).

Lipofectamine transfection was used for all experiments. Cells plated in 96-well plates were transiently transfected with the appropriate plasmid using Lipofectamine 2000 (Life Technologies), according to manufacturer's instructions. Following transfection, cell plates were returned to 37°C for 24 h. Chronic VX-809 treatment, where indicated, was started 24 h after transfection, and lasted 24 h.

The N-terminal YFP tag has been shown to only mildly alter function compared to the untagged channel (Langron et al., 2017), and others have shown that the GFP tag on the N-terminal, which we have used as a template for generating the YFP, does not significantly affect trafficking or function (Moyer et al., 1998; Vais et al., 2004). The pHTomato tag – inserted within the 4th extracellular loop – is also at a site known to be permissive for tag insertion in CFTR (Howard et al., 1995; Phuan et al., 2014; Veit et al., 2014; Hildebrandt et al., 2015).

YFP-CFTR fluorescence imaging

All imaging was carried out using ImageXpress (ImageXpress Micro XLS, Molecular Devices), an image-acquisition system equipped with wide-field inverted fluorescence microscope, CMOS camera and fluidics robotics. 96-well cell plates were held in an environmental chamber, at 37°C. YFP was imaged using a 20X objective, and excitation/emission filters 472 ± 30 nm and 520 ± 35 nm. For each plate, the laser intensity and exposure were optimised to achieve the highest possible fluorescence whilst avoiding both photobleaching and saturation (illumination intensity 100-150/225 c.d., and exposure 0.1 – 0.2 s). Images were taken at a frequency of 0.5 Hz.

To avoid systematic errors, and achieve a degree of randomization, conditions were not always tested in the same order. Blinding of these experiments was not feasible, given the resources available. However, the automated acquisition and rigorous analysis applied to the data effectively prevents subjective bias.

Before imaging, cells were washed twice with 100 µl standard buffer (140 mM NaCl, 4.7 mM KCl, 1.2 mM $MgCl_2$, 5 mM HEPES, 2.5 mM $CaCl_2$, 11 mM Glucose, pH 7.4). During imaging, after 20 s of baseline fluorescence acquisition, CFTR was activated in the absence of extracellular iodide (I^-), by addition of 50 µl standard buffer containing activating compounds. For steady-state experiments, after a further 230 s, 50 µl extracellular I^- was added (as standard buffer with 140 mM NaCl replaced with 400 mM NaI; resulting in final [I^-] of 100 mM). For experiments carried out to measure the rate of CFTR activation (see Fig. 3), the second addition occurred after a pre-incubation time of variable length (0 – 320 s). Activating compounds were included in the second addition so as not to alter final extracellular concentrations.

YFP-CFTR data analysis

Images were analysed using ImageJ (http://rsbweb.nih.gov/ij/). For each well, data were exported as a stack, with each time point represented by an image in the stack. Fluorescent areas corresponding to transfected cells were selected, before addition of I^-, using a threshold. Fluorescence was normalized to this maximal value, to allow comparison of fluorescence values between images, despite the variation in transfection efficiency and in other factors influencing absolute fluorescence values. CFTR activation was quantified by one of two methods, depending on the experiment type.

Quantification of non-stationary CFTR activity

For experiments used to measure the time course of CFTR activation (see Fig. 3), gating was quantified using the maximal rate of I^- influx, as described previously (Langron et al., 2017). Briefly, anion binding to YFP abolishes fluorescence in our system, so normalized fluorescence quantifies the proportion of unbound chromophores, and can be described by an equation including a Hill-Langmuir component:

$$F/F_{max} = 1 - \frac{[I^-]_{in}}{K_I + [I^-]_{in}} \qquad \text{Equation [1]}$$

where F/F_{max} is the normalized fluorescence, K_I is the dissociation constant for I^- binding to YFP (1.9 mM; Galietta et al., 2001a) and $[I^-]_{in}$ is the concentration of intracellular I^-.

Equation [1] can be rearranged to express $[I^-]_{in}$ as a function of F/F_{max}:

$$[I^-]_{in} = K_I \frac{1 - F/F_{max}}{F/F_{max}} \qquad \text{Equation [2]}$$

The maximal rate of I^- entry into cells ($\frac{d[I^-]_{in}}{dt}$, mM s^{-1}), immediately upon extracellular addition of I^-, was used to quantify CFTR activity.

To describe the time course of CFTR activation (e.g. Fig. 3B-D), the rate of I^- entry, as a function of pre-incubation time, was fit to a single exponential rise to maximum equation:

$$y = a(1 - e^{-\frac{t}{\tau}})$$

where *a* is the amplitude of the curve, *t* is the pre-incubation time and τ is the time constant of the exponential rise.

Quantification of CFTR activity at steady state

For steady-state experiments, a simple mathematical model was used to fit fluorescence quenching measurements and estimate CFTR conductance (See Supplementary Information SI1). Previously, a similar model was used to validate assumptions made when quantifying CFTR activity monitored during activation (Langron et al., 2017). In the current work, CFTR activation was first allowed to reach steady-state in the absence of I^-. Then, the changes in fluorescence values sampled in the 40 s following I^- addition, were fitted to the proportion of anion-free YFP chromophore predicted by the model (both normalized to the values read at the time point before I^- addition). Estimates for four free parameters are obtained: CFTR

conductance at steady-state (G_{CFTR}), membrane potential at steady-state (V_M), and conductance (G_{trans}) and time constant (τ_{trans}) of a transient, non-CFTR anion conductance. It was necessary to introduce the transient component to adequately describe the quenching time course. Endogenous anion permeabilities of the HEK293 cells, possibly triggered by a small (<10 mV) hyperpolarization predicted by the model upon I^- addition, likely underlie this component, because it was present in the absence of CFTR activation (average values of negative controls: G_{trans}: 13.2 nS ± 1.6 nS; τ_{trans}: 4.9 s ± 0.4 s, n = 19), its magnitude had no dependence on mutation, and was not correlated to CFTR conductance (r = 0.16, P = 0.5, Pearson's product moment correlation test). Furthermore, an anion conductance with a small amplitude, falling to zero within ~ 15 s of I^- addition was also detected in cells expressing G551D-CFTR (Supplementary Information SI2), i.e expressing a YFP-CFTR variant with a cellular distribution similar to WT-CFTR, but with negligible CFTR-associated conductance (Bompadre et al., 2007).

When CFTR conductance was low, the quenching time course allowed reliable estimation of all four free parameters, including G_{trans} and τ_{trans}. However, when CFTR conductance was high, due to the fast quenching rate, the time course did not provide enough information to uniquely identify all four parameters. Therefore, all quenching curves were fit in two ways: (1) with all four parameters estimated by fitting (Fig. 2, left panels, with G_{trans} constrained to < 25 nS, based on the distribution of estimates from negative controls), and (2) with G_{trans} and τ_{trans} fixed to the average obtained from negative controls, and only G_{CFTR} and V_M unconstrained (Fig. 2, right panels).

The sums of squared residuals (SSRs) obtained with the two alternative fits were then compared. If the fit obtained using method (1) was substantially better than that obtained using method (2) (>5-fold improvement in SSR), G_{CFTR} and V_M were estimated using method (1). This was most common in conditions in which CFTR conductance was low (Fig. 2A).

If the fit obtained using method (1) was not substantially better (<5-fold improvement in SSR), it was assumed that the parameters characterizing the transient component had the values measured for the negative controls, and G_{CFTR} and V_M were estimated using method (2) (Fig. 2B, also see Supplementary Information SI1). Preliminary studies had identified conditions in which quenching curves reached a steady state F/F_{max} within 2 s after I^- addition (corresponding to a G_{CFTR} greater than ~ 200 nS), i.e. quenching time course was too fast to be

followed with our current image-acquisition frequency (0.5 Hz). To avoid hitting this upper limit in our assay's dynamic range, a low forskolin concentration was used for basal activation.

Simulations and fits were run using MATLAB software, and the code is available upon request.

Quantitative description of concentration-response curves

Concentration-response curves were fitted using the Hill equation, with the Hill coefficient fixed to 1:

$$y = y_0 + \frac{a[L]}{EC_{50} + [L]}$$

where EC_{50} is the half maximal effective concentration, y_0 is the response measured in the absence of ligand, L is ligand and a is the amplitude of the curve.

CFTR-pHTomato fluorescence imaging

Before imaging, cells were incubated with Hoechst nuclear stain for 20 min at 37°C. Cells were then washed twice with 100 µl standard buffer (as above). During imaging, extracellular pH was changed using the addition of 50 µl pH 6 buffer (as standard buffer, with 5 mM HEPES replaced with 10 mM 2-(Nmorpholino)ethanesulfonic acid (MES): final [MES] 3.3 mM, final extracellular value approximately pH 6.5), followed by 50 µl pH 9 buffer (as standard buffer, with 5 mM HEPES replaced with 100 mM Tris: final [Tris] 25 mM, extracellular approximately pH 8.8). The change in fluorescence upon pH change (from pH 6.5 to pH 8.8) was used to quantify membrane-localised CFTR.

pHTomato images were taken at a frequency of 0.5 Hz, using excitation/emission filters 531 ± 20 nm and 592 ± 20 nm. Single eGFP and Hoechst nuclear stain images were also acquired for each well, using excitation/emission filters 472 ± 30 and 520 ± 35 nm, and 377 ± 25 and 447 ± 30 nm, respectively.

CFTR-pHTomato data analysis

Analysis was carried out as previously described (Langron et al., 2017). In brief, regions corresponding to transfected cells were selected based on eGFP fluorescence, and for each selected region, the mean eGFP fluorescence (F_{green}) was used to normalize the mean

pHTomato fluorescence (F_{red}), to allow for differences in transfection efficiency. A weighted average was then obtained, with each region weighted by cell count:

$$F_{pHTomato} = \frac{\sum\left(\frac{F_{red}}{F_{green}} cell\ count\right)}{\sum(cell\ count)}$$

The change in $F_{pHTomato}$ upon changing the extracellular buffer from pH 6.5 to pH 8.8 was used to quantify membrane-localised CFTR (ΔF_M). ΔF_M measurements were normalized to within-plate WT-CFTR controls, to allow comparison of fluorescence changes between plates.

Statistical analysis

All average plots including error bars represent mean ± SEM. No pattern or abnormality was noticed, when considering individual measurements, that is not obvious in the data as presented. Comparisons were made using a non-parametric Kruskal-Wallis one-way ANOVA, followed, when a difference between groups was identified (F achieved $P < 0.05$), by a post-hoc Dunn's test (for comparison to a control group). Significance indicates $P < 0.05$. All statistical analysis was carried out using SigmaPlot v11 (Systat Software). The data and statistical analysis comply with the recommendations on experimental design and analysis in pharmacology (Curtis et al., 2015), and its update (Curtis et al., 2018).

Note on nomenclature

All measurements presented in this paper were obtained from HEK293 cells expressing CFTR fusions with fluorescent proteins. In order not to overly complicate nomenclature, only the mutation is mentioned when referring to a CFTR version, omitting the fused fluorescent protein (e.g. K1250R-CFTR, rather than K1250R-YFP-CFTR), unless the focus of the sentence/paragraph is on the assay, rather than on the CFTR version (YFP-CFTR assay).

Key protein targets and ligands in this article are hyperlinked to corresponding entries in http://www.guidetopharmacology.org, the common portal for data from the IUPHAR/BPS Guide to PHARMACOLOGY (Harding et al., 2018), and are permanently archived in the Concise Guide to PHARMACOLOGY 2017/18 (Alexander et al., 2017).

Results

YFP-CFTR protocol optimisation for steady-state measurements

CFTR activity was measured using a YFP-CFTR fusion protein (Langron et al., 2017), in which halide-sensitive YFP (H148Q/I152L; Galietta et al., 2001a) is tagged to the N-terminal of CFTR. A higher affinity for I^- compared to Cl^- (1.9 mM K_I vs. 85 mM K_{Cl}; Galietta et al., 2001a) allows the use of Cl^-/I^- exchange protocols to investigate CFTR ion channel function (e.g. Galietta et al., 2001b).

In most of this paper, YFP-CFTR, expressed in HEK293 cells, is first fully activated by forskolin in the absence of extracellular I^-. Forskolin, by activating adenylate cyclase, results in phosphorylation and activation of YFP-CFTR. Upon addition of extracellular I^-, I^- enters the cell via open anion channels and, as the cytosolic $[I^-]$ increases, the proportion of YFP chromophores in which the anion-binding site is unoccupied falls, causing a fall in YFP fluorescence (e.g. Fig. 2). This protocol, by bypassing the activation time course, minimizes the number of free parameters required to describe the YFP quenching time course (cf. Langron et al., 2017).

However, we first needed to determine the length of the forskolin pre-incubation required for CFTR to reach steady-state activation. Therefore, the pre-incubation time interval (Fig. 3A, blue arrow) was varied from 0 s to 320 s, after which 100 mM I^- was added extracellularly (Fig. 3A, red bar).

In the presence of 1 µM and 10 µM forskolin, WT-CFTR reached maximal activation after 150-200 s (Fig. 3B). To confirm that D1370N, K1250R and K464A mutations did not greatly alter the rate of CFTR activation, we constructed comparable activation curves for each genotype (Fig. 3C and 3D): the activation time-constants were not significantly altered by the mutations (Fig. 3B-D, see also Supplementary Information SI3). To limit the length of experiments, whilst also ensuring CFTR function was measured close to steady-state, 230 s was chosen as a pre-incubation time for all further experiments (Fig. 3B-D, dashed line).

Membrane exposure of CFTR

CFTR conductance in the YFP-CFTR assay depends on the number of channels at the membrane, as well as on gating and permeation properties of individual channels. To deconvolve mutation effects on one or the other of these quantities, we require information on

how the mutation in question affects plasma membrane density, when CFTR is expressed in HEK293 cells. For instance, we see that the maximal I^--entry rate for K464A-CFTR in 10 μM forskolin is dramatically reduced compared to that for WT-CFTR (Fig. 3D vs. 3B). How much of this is due to a trafficking (Thibodeau et al., 2010), and how much to a gating (Vergani et al., 2003; Csanády et al., 2010) defect?

To answer such questions, membrane exposure of CFTR was measured using the CFTR-pHTomato fusion protein (Langron et al., 2017). In this probe, pHTomato (Li and Tsien, 2012) an acid-sensitive red fluorescent protein, is tagged to the fourth extracellular loop of CFTR (known to be an insertion-permissive site; Howard et al., 1995; Hildebrandt et al., 2015). Only for CFTR-pHTomato molecules located at the plasma membrane, is pHTomato exposed to the extracellular buffer. Alkalinizing the extracellular pH (from pH 6.5 to pH 8.8, which corresponds to a change in pHTomato normalized fluorescence intensity approximately from 0.1 to 0.9; Li and Tsien, 2012) causes a fluorescence increase. This fluorescence change is used to quantify the amount of CFTR on the membrane.

The D1370N and K1250R mutations did not significantly change membrane exposure compared to WT-CFTR (Fig. 4A). The K464A-CFTR trafficking defect (Thibodeau et al., 2010), however, is severe in this system, resulting in only ~10% K464A-CFTR reaching the membrane compared with WT-CFTR (Fig. 4B). 24 h treatment with corrector compound VX-809 partially corrects trafficking (membrane exposure reaching ~35% of WT-CFTR; Fig. 4B).

A very similar trafficking defect, which is partially corrected by VX-809, is also found for the K464A/K1250R double mutant (Fig. 4C). In all further experiments, K464A-CFTR and K464A/K1250R-CFTR were treated with 10 μM VX-809 for 24 h before imaging, to increase the magnitude of CFTR-mediated conductance allowing more accurate functional studies.

Potentiation by VX-770

The conductance of CFTR at steady state (estimated by fitting the YFP quenching time course following I^- addition to the change in unoccupied chromophores predicted by a simple mathematical model, see Methods and Supplementary Information SI1), was used to compare CFTR function in different genotypes/conditions.

CFTR conductance was estimated after activation with increasing concentrations of forskolin, and concentration-response curves were constructed (Fig. 5) to characterize constructs and identify a suitable forskolin concentration at which to study potentiation.

Maximal CFTR conductance is smaller for constructs including the K464A mutation (Fig. 5C-D vs. Fig. 5A-B), probably reflecting reduced membrane exposure (Fig. 4) and known gating impairment (Carson et al., 1995; Vergani et al., 2003; Csanády et al., 2010). Fitting also provides estimates of membrane potential, V_M, once steady-state activation of CFTR is reached. As expected, forskolin causes a concentration-dependent depolarisation of cells expressing CFTR, producing concentration-response curves (Fig. SI4) comparable to those shown in Fig. 5, although estimates for V_M appear less well defined (e.g. more sensitive to initial parameter setting), than those for G_{CFTR}. WT-CFTR, D1370N-CFTR, K1250R-CFTR and K464A-CFTR G_{CFTR} curves are all similarly positioned on the forskolin concentration axis (EC_{50} values in the low micromolar range; no significant difference, $P > 0.05$), suggesting similar sensitivity to phosphorylation. The K464A/K1250R-CFTR G_{CFTR} curve is shifted slightly compared to WT-CFTR ($P = 0.03$), suggesting a possible slight increase in sensitivity to cAMP/phosphorylation.

300 nM forskolin (between EC_{10} and EC_{40} for all genotypes) was chosen to provide a low level of phosphorylation, low enough for fully potentiated conditions to remain within the dynamic range of our assay. For K464A/K1250R-CFTR (for which 300 nM forskolin is ~EC_{40} on the G_{CFTR}-[forskolin] curve; Fig. 5D), a lower forskolin concentration of 100 nM (~EC_{20}) was also used.

YFP-CFTR quenching was therefore measured at increasing concentrations of VX-770 at these low phosphorylation levels, and fitting yielded data points to construct [VX-770]-G_{CFTR} (Fig. 6) curves (see also [VX-770]-V_M curves, Fig. SI5). VX-770 strongly potentiates WT-CFTR and the two non-hydrolytic mutants (Fig. 6A-B, Fig. SI5A-B and Fig. 7). Cells expressing K464A-CFTR were treated for 24 h with 10 µM VX-809, to increase membrane exposure (see Fig. 4B). Although maximal quenching rates (and therefore estimated maximal G_{CFTR}, Fig. 6C) are lower compared to WT-CFTR, K464A G_{CFTR} is also low in basal conditions, such that VX-770 still induces large potentiation (Fig. 6C and Fig. 7, see also Fig. SI5C). Sensitivity to VX-770 was not altered by K1250R, D1370N or K464A mutations ($P = 0.4$).

To eliminate effects due to VX-770 interaction with the rarely frequented post-hydrolytic O_2 conformation of K464A-CFTR, the K1250R mutation was also introduced in a K464A-CFTR background. For both 100 nM and 300 nM forskolin concentrations (see above

and Fig. 5D), changes in K464A/K1250R-CFTR activity due to VX-770 action are comparable to those seen for K464A-CFTR (Fig. 6C-D, Fig. SI5C-D and Fig. 7).

Discussion

VX-770 has been shown to potentiate a very large number of mutant CFTR versions (e.g. Yu et al., 2012; Van Goor et al., 2014), and evidence is accumulating on the clinical benefits provided to patients (Accurso et al., 2010; Bessonova et al., 2018). However, the effects of many of these mutations on CFTR gating have not been characterized in detail, and even less is known about how VX-770 mends their gating defect. In this study we use mutants that have been studied extensively with electrophysiological techniques, as a tool to investigate VX-770 mechanism. Such mutants, showing relatively minor alterations of P_o (< 3-fold change), are thought to visit open channel states structurally equivalent to those visited by WT-CFTR, but to progress from pre-hydrolytic O_1 to post-hydrolytic O_2 state rarely, or not at all. Quantitatively comparing the magnitude of VX-770 potentiation of WT and of a number of such mutants, while minimizing uncontrolled variables, allows us to make general inferences on the mechanism of action of VX-770 on CFTR, likely to be valid for many gating mutants. A better mechanistic understanding of how VX-770 affects CFTR function could guide the development of improved genotype-specific CFTR-targeting drugs in the future.

VX-770 potentiation involves stabilization of pre-hydrolytic open state O_1

To investigate VX-770's mechanism of action, we used two non-hydrolytic CFTR mutants: D1370N-CFTR and K1250R-CFTR. These mutations likely impair catalytic activity at site 2, and electrophysiological evidence is consistent with channels toggling, at saturating [ATP], between ATP-bound closed, C, and pre-hydrolytic O_1 states, without ever entering the O_2 state (Gunderson and Kopito, 1995; Vergani et al., 2003, 2005; Csanády et al., 2010). Due to the similar membrane exposure (Fig. 4) and single-channel conductance of WT-CFTR and non-hydrolytic CFTR mutants, similar G_{CFTR} values reflect similar P_o values. Our G_{CFTR} measurements (Fig. 3B-C, Fig. 5A-B) are largely consistent with what is known for these mutants obtained from patch-clamp experiments (Vergani et al., 2003, 2005; Bompadre et al., 2005; Csanády et al., 2010).

Because in non-hydrolytic mutants opening and closing are forward and backwards transitions along the same kinetic pathway ($C_1 \leftrightarrow O_1$), the only mechanism by which VX-770 can increase P_o in these mutants is via stabilization of the O_1 state with respect to C. Merely stabilizing the opening transition state would cause an increase in opening rate with a concurrent increase in closing rate, and therefore result in no net change in P_o.

The fact that WT-CFTR and non-hydrolytic mutants are similarly potentiated by VX-770 (~ 10-fold, Fig. 7) suggests that in WT-CFTR too VX-770 potentiates gating mainly by slowing closing rate. This is most simply explained by a selective stabilization of the O_1 state by VX-770: whereas O_1 stabilization slows closure in non-hydrolytic mutants by slowing step $O_1 \rightarrow C_1$ (rate k_{-1}; Fig. 1), in WT-CFTR it does so by slowing step $O_1 \rightarrow O_2$ (rate k_1; Fig. 1). In the absence of substantial effects on the stabilities of the transition states for the above two steps, selective stabilization of the O_1 ground state will similarly slow closure of WT and non-hydrolytic mutants, while leaving opening rate unaffected (consistent with Jih and Hwang, 2013 at millimolar [ATP]). However, more complex scenarios are also possible.

Similarity of VX-770's effect on the CFTR versions tested here strongly suggests that stabilization of the post-hydrolytic O_2 state (Jih and Hwang, 2013), likely never visited by non-hydrolytic mutants gating in millimolar [ATP], and visited rarely by K464A-CFTR (Csanady et al., 2010), is not fundamental for VX-770 action. Burst duration distributions of D1370N-CFTR mutants show a monotonic decay, with no evidence of a negative fractional amplitude exponential component, consistent with virtually all bursts closing non-hydrolytically. In contrast, burst duration distributions of K464A mutants include a significant negative exponential component, a distinctive paucity of events accumulating in the briefest burst duration bins, reflecting the rare bursts terminating through hydrolysis (Csanady et al., 2010). Biochemical studies measured a residual ATPase activity in K464A-CFTR of approximately 10% of that of WT-CFTR (Ramjeesingh et al., 1999), suggesting that any minute residual ATPase activity in D1370N-CFTR is well below this level. To result in equal VX-770 potentiation on all CFTR versions tested here, an action of VX-770 on O_2 would require the magnitude of stabilization of these post-hydrolytic events to be roughly inversely related to their differing frequency, resulting in a similar overall potentiation of WT and mutants. This interpretation seems much less likely than a simple, similar action on O_1.

VX-770 potentiation and site 1 conformational dynamics.

It should be noted that cells expressing K464A-CFTR and K464A/K1250R-CFTR were treated with VX-809, to increase membrane expression and allow functional studies. It cannot be ruled out that VX-809 altered the response to VX-770 in these CFTR variants. However, the similarity of the effects of VX-770 on these and on other (non VX-809-treated) variants is consistent with there being little drug-drug interaction for the acute responses measured here.

Recent results suggest that conformational changes around the ATP bound at site 1, occurring relatively late along the reaction coordinate for channel opening, contribute substantially to the stabilization of the pre-hydrolytic open state O_1, preventing the reversal of the opening transition and therefore assuring that WT-CFTR gating is coupled to the hydrolytic cycle at the NBDs (Sorum et al., 2015). The K464A mutation, removing a lysine side chain crucial for interactions with ATP at site 1, itself destabilizes the pre-hydrolytic open state O_1, with respect to the transition state for opening (Powe Jr et al., 2002; Vergani et al., 2003; Bompadre et al., 2005; Csanády et al., 2010), most likely by interfering with these conformational changes at site 1. The fact that VX-770 potentiation is not greatly affected by the K464A mutation (~ 10-fold potentiation, as seen in WT-CFTR, Fig.7) suggests that the effects of the mutation and of the drug are additive, i.e., that VX-770 binding does not stabilize O_1 by changing the protein dynamics at site 1. Other conformational changes occurring during the opening of the channel, while the protein relaxes from the strained transition state to the open ground state (O_1) must be altered by binding of VX-770 to the protein. The extremely hydrophobic physicochemical properties of the drug argue for drug binding in the transmembrane domains, possibly on areas exposed to the lipid bilayer (Jih et al., 2013). More studies are required to further characterize the molecular determinants of VX-770's action.

VX-770 has been shown to cause a substantial increase in opening rate of F508del-CFTR (Kopeikin et al., 2014). Like K464A, the F508del mutation also destabilizes the pre-hydrolytic O_1 state (Jih et al., 2011). However, gating of F508del-CFTR is likely largely hydrolytic, as demonstrated by the strong potentiation by NPPB (Csanády and Töröcsik, 2014 but cf. Lin et al., 2016), and by almost 100-fold slowing of F508del-CFTR closing rate by the E1371S mutation (Kopeikin et al., 2014). The apparent discrepancy between the effect of VX-770 on WT-CFTR and the mutants investigated in this paper vs. on F508del-CFTR might be related to the very severe defect in opening measured in the latter mutant (e.g. Miki et al., 2010; Cai et al., 2015). While the opening transition of WT, K1250R, D1370N and K464A mutants (for which measured opening rates at saturating [ATP] vary less than 3-fold: Vergani et al., 2003; Csanady et al., 2010; Vergani et al., 2005) likely occurs via similar structural conformational changes, the energetic landscape visited during opening by F508del-CFTR channels might be quite distinct, with bound VX-770 providing a substantially facilitated pathway.

Mutations do not affect VX-770 apparent affinity for CFTR

None of the mutations studied here caused any significant shift in [VX-770]-G_{CFTR} concentration-response curves. Because mutation effects on P_o are minor, this result suggests that the mutations do not differentially affect VX-770-bound and unbound channels.

Conclusion

VX-770 is an effective potentiator used to treat CF. As well as potentiating WT-CFTR, which closes via a hydrolytic pathway, VX-770 potentiates mutants which gate at equilibrium (Van Goor et al., 2009; Eckford et al., 2012; Yeh et al., 2015). Our data, demonstrating similar potentiation of a number of gating mutants in which hydrolysis is impaired to varying degrees, are consistent with VX-770 potentiating CFTR by stabilizing the pre-hydrolytic O_1 state.

As structural information on the closed (Zhang and Chen, 2016; Liu et al., 2017; Zhang et al., 2017) and open CFTR channel becomes available, a better understanding of the conformational changes altered by VX-770 and other drugs will be important for the development of improved, and genotype-specific, treatment for CF patients. Our assay - with which researchers can rapidly obtain quantitative information on how drugs alter CFTR ion channel function for many CFTR variants, in near-native cellular conditions - provides a robust and adaptable tool for further investigations.

Author Contributions

Experiments were conceived and designed by EL and PV. EL carried out the molecular biology and ran the fluorescence assay acquisition and image analysis. SP implemented the mathematical model in the MATLAB environment. Manuscript was written by EL and PV. All authors read and commented on the final draft of the manuscript.

Acknowledgements

EL was supported by grant 15UCL04, funded by the Sparks charity and Cystic Fibrosis Trust (Venture and Innovation Award). SP was supported by grant SRC005 funded by the Cystic Fibrosis Trust. We thank Dr László Csanády, Semmelweis University, for very interesting discussions.

Conflict of interest declaration

The authors declare no conflicts of interest

References

Accurso, F.J., Rowe, S.M., Clancy, J.P., Boyle, M.P., Dunitz, J.M., Durie, P.R., et al. (2010). Effect of VX-770 in Persons with Cystic Fibrosis and the G155D-CFTR Mutation. N. Engl. J. Med. *363*: 1991–2003.

Bessonova, L., Volkova, N., Higgins, M., Bengtsson, L., Tian, S., Simard, C., et al. (2018). Data from the US and UK cystic fibrosis registries support disease modification by CFTR modulation with ivacaftor. Thorax. Published Online First: 10 May 2018. doi: 10.1136/thoraxjnl-2017-210394

Bompadre, S.G., Cho, J.H., Wang, X., Zou, X., Sohma, Y., Li, M., et al. (2005). CFTR gating II: Effects of nucleotide binding on the stability of open states. J. Gen. Physiol. *125*: 377–394.

Bompadre, S.G., Sohma, Y., Li, M., and Hwang, T.-C. (2007). G551D and G1349D, two CF-associated mutations in the signature sequences of CFTR, exhibit distinct gating defects. J. Gen. Physiol. *129*: 285–298.

Cai, Z., Palmai-Pallag, T., Khuituan, P., Mutolo, M.J., Boinot, C., Liu, B., et al. (2015). Impact of the F508del mutation on ovine CFTR, a Cl^- channel with enhanced conductance and ATP-dependent gating. J. Physiol. *593*: 2427–2446.

Carson, M.R., Travis, S.M., and Welsh, M.J. (1995). The Two Nucleotide-binding Domains of Cystic Fibrosis Transmembrane Conductance Regulator (CFTR) Have Distinct Functions in Controlling Channel Activity. J. Biol. Chem. *270*: 1711–1717.

Chang, X.B., Tabcharani, J.A., Hou, Y.X., Jensen, T.J., Kartner, N., Alon, N., et al. (1993). Protein kinase A (PKA) still activates CFTR chloride channel after mutagenesis of all 10 PKA consensus phosphorylation sites. J. Biol. Chem. *268*: 11304–11311.

Chaves, L.A.P., and Gadsby, D.C. (2015). Cysteine accessibility probes timing and extent of NBD separation along the dimer interface in gating CFTR channels. J. Gen. Physiol. *145*: 261–283.

Chen, J., Lu, G., Lin, J., Davidson, A.L., and Quiocho, F. A. (2003). A tweezers-like motion of the ATP-binding cassette dimer in an ABC transport cycle. Mol. Cell *12*: 651–661.

Csanady, L., Mihalyi, C., Szollosi, A., Torocsik, B., and Vergani, P. (2013). Conformational changes in the catalytically inactive nucleotide-binding site of CFTR. J. Gen. Physiol. *142*: 61–73.

Csanády, L., and Töröcsik, B. (2014). Structure-activity analysis of a CFTR channel potentiator: Distinct molecular parts underlie dual gating effects. J. Gen. Physiol. *144*: 321–336.

Csanády, L., Vergani, P., and Gadsby, D.C. (2010). Strict coupling between CFTR's catalytic cycle and gating of its Cl- ion pore revealed by distributions of open channel burst durations. Proc. Natl. Acad. Sci. U. S. A. *107*: 1241–1246.

Curtis, M., Bond, R., Spina, D., Ahluwalia, A., Alexander, S., Giembycz, M., et al. (2015). Experimental design and analysis and their reporting: new guidance for publication in BJP. Br. J. Pharmacol. *172*: 3461–3471.

Curtis, M., Alexander, S., Cirino, G., Docherty, J.R., George, C.H., Giembycz, M. et al.

(2018). Experimental design and analysis and their reporting II: updated and simplified guidance for authors and peer reviewers. Br J Pharmacol. *175*: 987-993.

Davies, J.C., Wainwright, C.E., Canny, G.J., Chilvers, M.A., Howenstine, M.S., Munck, A., et al. (2013). Efficacy and safety of Ivacaftor in patients aged 6 to 11 years with cystic fibrosis with a G155D mutation. Am. J. Respir. Crit. Care Med. *187*: 1219–1225.

Eckford, P.D.W., Li, C., Ramjeesingh, M., and Bear, C.E. (2012). Cystic fibrosis transmembrane conductance regulator (CFTR) potentiator VX-770 (ivacaftor) opens the defective channel gate of mutant CFTR in a phosphorylation-dependent but ATP-independent manner. J. Biol. Chem. *287*: 36639–36649.

Galietta, L.J., Haggie, P.M., and Verkman, A.S. (2001a). Green fluorescent protein-based halide indicators with improved chloride and iodide affinities. FEBS Lett. *499*: 220–224.

Galietta, L. V, Jayaraman, S., and Verkman, A.S. (2001b). Cell-based assay for high-throughput quantitative screening of CFTR chloride transport agonists. Am. J. Physiol. Cell Physiol. *281*: C1734-42.

Gunderson, K.L., and Kopito, R.R. (1995). Conformational states of CFTR associated with channel gating: the role ATP binding and hydrolysis. Cell *82*: 231–239.

Harding SD, Sharman JL, Faccenda E, Southan C, Pawson AJ, Ireland S *et al.* (2018). The IUPHAR/BPS Guide to PHARMACOLOGY in 2018: updates and expansion to encompass the new guide to IMMUNOPHARMACOLOGY. Nucl Acids Res *46*: D1091-D1106.

Hildebrandt, E., Ding, H., Mulky, A., Dai, Q., Aleksandrov, A.A., Bajrami, B., et al. (2015). A Stable Human-Cell System Overexpressing Cystic Fibrosis Transmembrane Conductance Regulator Recombinant Protein at the Cell Surface. Mol. Biotechnol. *57*: 391–405.

Howard, M., DuVall, M.D., Devor, D.C., Dong, J.Y., Henze, K., and Frizzell, R.A. (1995). Epitope tagging permits cell surface detection of functional CFTR. Am. J. Physiol. *269*: C1565-1576.

Jih, K.-Y., and Hwang, T.-C. (2013). Vx-770 potentiates CFTR function by promoting decoupling between the gating cycle and ATP hydrolysis cycle. Proc. Natl. Acad. Sci. U. S. A. *110*: 4404–9.

Jih, K.-Y., Li, M., Hwang, T.-C., and Bompadre, S.G. (2011). The most common cystic fibrosis-associated mutation destabilizes the dimeric state of the nucleotide-binding domains of CFTR. J. Physiol. *589*: 2719–2731.

Kopeikin, Z., Yuksek, Z., Yang, H.-Y., and Bompadre, S.G. (2014). Combined effects of VX-770 and VX-809 on several functional abnormalities of F508del-CFTR channels. J. Cyst. Fibros. *13*: 508–14.

Langron, E., Simone, M.I., Delalande, C.M.S., Reymond, J.L., Selwood, D.L., and Vergani, P. (2017). Improved fluorescence assays to measure the defects associated with F508del-CFTR allow identification of new active compounds. Br. J. Pharmacol. *174*: 525–539.

Lerner-Marmarosh, N., Gimi, K., Urbatsch, I.L., Gros, P., and Senior, A.E. (1999). Large Scale Purification of Detergent-soluble P-glycoprotein fromPichia pastoris Cells and Characterization of Nucleotide Binding Properties of Wild-type, Walker A, and Walker B Mutant Proteins. J. Biol. Chem. *274*: 34711–34718.

Li, Y., and Tsien, R.W. (2012). pHTomato, a red, genetically encoded indicator that enables multiplex interrogation of synaptic activity. Nat. Neurosci. *15*: 1047–1053.

Lin, W.-Y., Jih, K.-Y., and Hwang, T.-C. (2014). A single amino acid substitution in CFTR converts ATP to an inhibitory ligand. J. Gen. Physiol. *144*: 311–320.

Lin, W.-Y., Sohma, Y., and Hwang, T.-C. (2016). Synergistic Potentiation of CFTR gating by two chemically distinct potentiators, Ivacaftor (VX-770) and NPPB. Mol. Pharmacol. *90:* 275–285.

Liu, F., Zhang, Z., Csanády, L., Gadsby, D.C., and Chen, J. (2017). Molecular Structure of the Human CFTR Ion Channel. Cell *169*: 85–92.

Miki, H., Zhou, Z., Li, M., Hwang, T.-C., and Bompadre, S.G. (2010). Potentiation of disease-associated cystic fibrosis transmembrane conductance regulator mutants by hydrolyzable ATP analogs. J. Biol. Chem. *285*: 19967–19975.

Moyer, B.D., Loffing, J., Schwiebert, E.M., Loffing-Cueni, D., Halpin, P.A., Karlson, K.H., et al. (1998). Membrane Trafficking of the Cystic Fibrosis Gene Product , Cystic Fibrosis Transmembrane Conductance Regulator , Tagged with Green Fluorescent Protein in Madin-Darby Canine Kidney Cells. J. Biol. Chem. *273*: 21759–21768.

Phuan, P.-W., Veit, G., Tan, J., Roldan, A., Finkbeiner, W.E., Lukacs, G., et al. (2014). Synergy-based Small-Molecule Screen Using a Human Lung Epithelial Cell Line Yields F508-CFTR Correctors that Augment VX-809 Maximal Efficacy. Mol. Pharmacol. *86*: 42–51.

Powe Jr, A.C., Al-nakkash, L., Li, M., and Hwang, T. (2002). Mutation of Walker-A lysine 464 in cystic fibrosis transmembrane conductance regulator reveals functional interaction between its nucleotide-binding domains. J. Physiol. *539*: 333–346.

Rai, V., Gaur, M., Shukla, S., Shukla, S., Ambudkar, S. V, Komath, S.S., et al. (2006). Conserved Asp327 of Walker B motif in the N-terminal nucleotide binding domain (NBD-1) of Cdr1p of Candida albicans has acquired a new role in ATP hydrolysis. Biochemistry *45*: 14726–14739.

Ramjeesingh, M., Li, C., Garami, E., Huan, L.J., Galley, K., Wang, Y., et al. (1999). Walker mutations reveal loose relationship between catalytic and channel-gating activities of purified CFTR (cystic fibrosis transmembrane conductance regulator). Biochemistry *38*: 1463–1468.

Ramsey, B.W., Jane, D., McElvaney, N.G., Tullis, E., Bell, S.C., Dřevínek, P., et al. (2011). A CFTR Potentiator in Patients with Cystic Fibrosis and the G155D mutation. N. Engl. J. Med. *365*: 1663–1672.

Riordan, J.R., Rommens, J.M., Kerem, B., Alon, N., Rozmahel, R., Grzelczak, Z., et al. (1989). Identification of the cystic fibrosis gene: cloning and characterization of complementary DNA. Science *245*: 1066–1073.

Smith, P.C., Karpowich, N., Millen, L., Moody, J.E., Rosen, J., Thomas, P.J., et al. (2002). ATP binding to the motor domain from an ABC transporter drives formation of a nucleotide sandwich dimer. Mol. Cell *10*: 139–149.

Sorum, B., Czégé, D., and Csanády, L. (2015). Timing of CFTR Pore Opening and Structure of Its Transition State. Cell *163*: 724–733.

Thibodeau, P.H., Richardson, J.M., Wang, W., Millen, L., Watson, J., Mendoza, J.L., et al. (2010). The cystic fibrosis-causing mutation deltaF508 affects multiple steps in cystic fibrosis transmembrane conductance regulator biogenesis. J. Biol. Chem. *285*: 35825–35835.

Tsai, M.-F., Li, M., and Hwang, T.-C. (2010). Stable ATP binding mediated by a partial NBD dimer of the CFTR chloride channel. J. Gen. Physiol. *135*: 399–414.

Urbatsch, I.L., Sankaran, B., Weber, J., and Senior, A.E. (1995). P-glycoprotein is stably inhibited by vandate-induced trapping of nucleotide at a single catalytic site. J. Biol. Chem. *270*: 19383–19390.

Vais, H., Gao, G.-P., Yang, M., Tran, P., Louboutin, J.-P., Somanathan, S., et al. (2004). Novel adenoviral vectors coding for GFP-tagged wtCFTR and deltaF508-CFTR: characterization of expression and electrophysiological properties in A549 cells. Pflugers Arch. *449*: 278–287.

Van Goor, F., Hadida, S., Grootenhuis, P.D.J., Burton, B., Cao, D., Neuberger, T., et al. (2009). Rescue of CF airway epithelial cell function in vitro by a CFTR potentiator, VX-770. Proc. Natl. Acad. Sci. U. S. A. *106*: 18825–18830.

Van Goor, F., Yu, H., Burton, B., and Hoffman, B.J. (2014). Effect of ivacaftor on CFTR forms with missense mutations associated with defects in protein processing or function. J. Cyst. Fibros. *13*: 29–36.

Veit, G., Avramescu, R.G., Perdomo, D., Phuan, P.-W., Bagdany, M., Apaja, P.M., et al. (2014). Some gating potentiators, including VX-770, diminish F508-CFTR functional expression. Sci. Transl. Med. *6*: 246ra97.

Vergani, P., Lockless, S.W., Nairn, A.C., and Gadsby, D.C. (2005). CFTR channel opening by ATP-driven tight dimerization of its nucleotide-binding domains. Nature *433*: 876–880.

Vergani, P., Nairn, A.C., and Gadsby, D.C. (2003). On the Mechanism of MgATP-dependent Gating of CFTR Cl- Channels. J. Gen. Physiol. *120*: 17–36.

Walker, J.E., Saraste, M., Runswick, M., and Gay, N.J. (1982). Distantly related sequences in the alpha- and beta-subunits of ATP synthase, myosin, kinases and other ATP-requiring enzymes and a common nucleotide binding fold. EMBO J. *1*: 945–951.

Yeh, H.-I., Yeh, J.-T., and Hwang, T.-C. (2015). Modulation of CFTR gating by permeant ions. J. Gen. Physiol. *145*: 47–60.

Yu, H., Burton, B., Huang, C.-J., Worley, J., Cao, D., Johnson, J.P., et al. (2012). Ivacaftor potentiation of multiple CFTR channels with gating mutations. J. Cyst. Fibros. *11*: 237–245.

Yuan, Y.R., Blecker, S., Martsinkevich, O., Millen, L., Thomas, P.J., and Hunt, J.F. (2001). The crystal structure of the MJ0796 ATP-binding cassette. Implications for the structural consequences of ATP hydrolysis in the active site of an ABC transporter. J. Biol. Chem. *276*: 32313–32321.

Zhang, Z., and Chen, J. (2016). Atomic structure of the Cystic Fibrosis Transmembrane Conductance Regulator. Cell *167*: 1586–1597.

Zhang, Z., Liu, F., and Chen, J. (2017). Conformational Changes of CFTR upon Phosphorylation and ATP Binding. Cell *170*: 483–491.

Figure 1

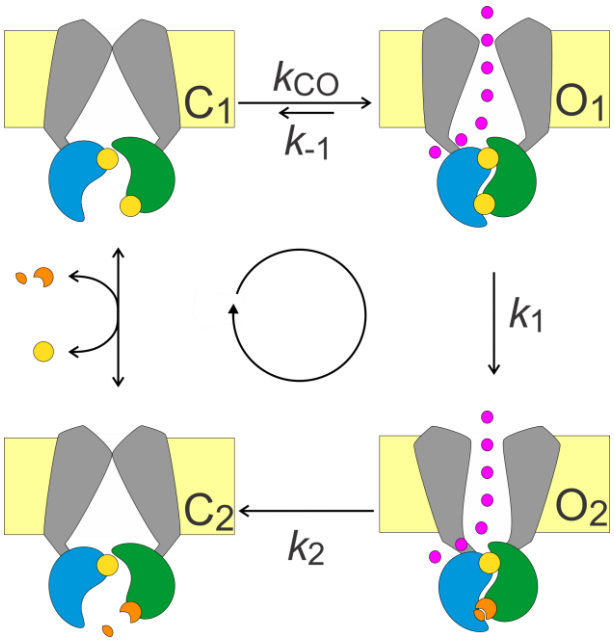

Figure 2

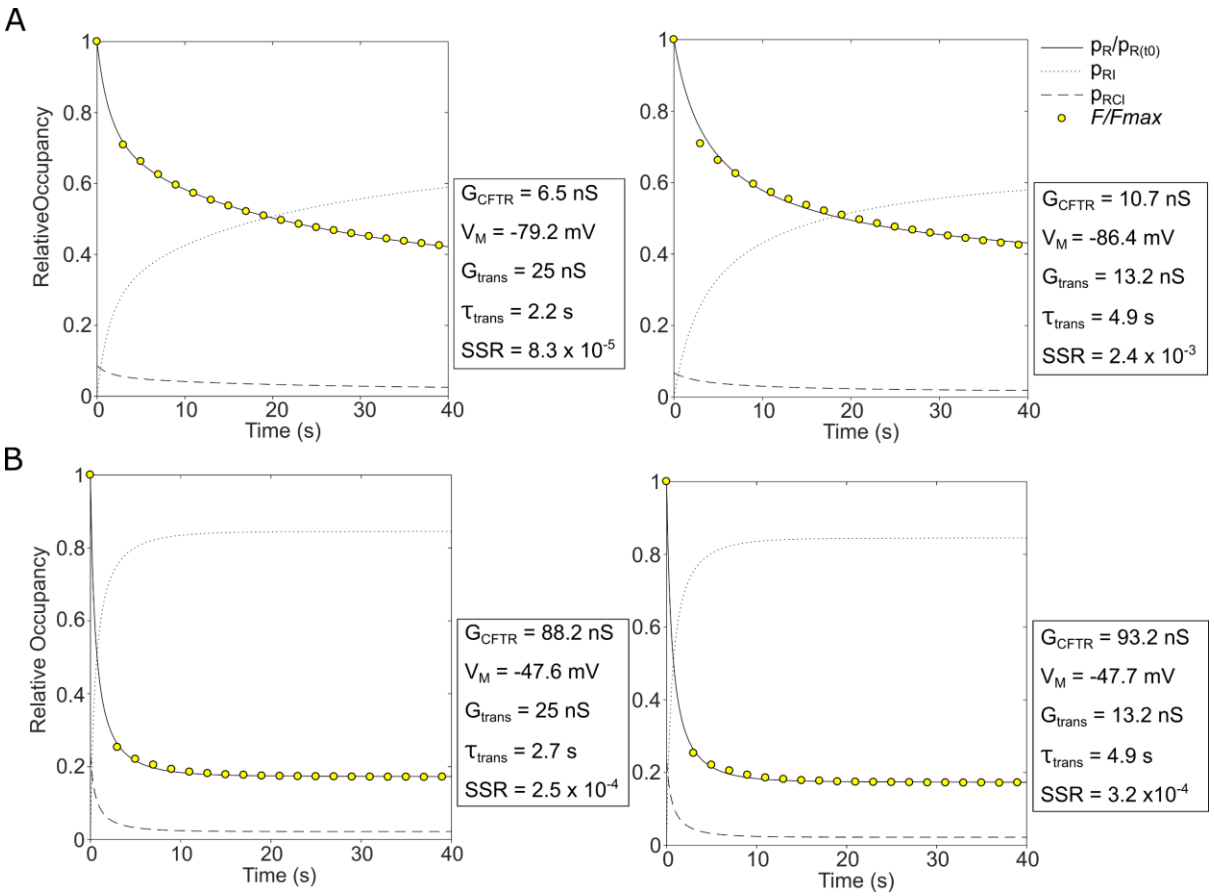
A
RelativeOccupancy
Time (s)
G_{CFTR} = 6.5 nS
V_M = -79.2 mV
G_{trans} = 25 nS
τ_{trans} = 2.2 s
SSR = 8.3 x 10^{-5}
G_{CFTR} = 10.7 nS
V_M = -86.4 mV
G_{trans} = 13.2 nS
τ_{trans} = 4.9 s
SSR = 2.4 x 10^{-3}
$p_R/p_{R(t0)}$
p_{RI}
p_{RCI}
F/Fmax
B
Relative Occupancy
Time (s)
G_{CFTR} = 88.2 nS
V_M = -47.6 mV
G_{trans} = 25 nS
τ_{trans} = 2.7 s
SSR = 2.5 x 10^{-4}
G_{CFTR} = 93.2 nS
V_M = -47.7 mV
G_{trans} = 13.2 nS
τ_{trans} = 4.9 s
SSR = 3.2 x10^{-4}

Figure 3

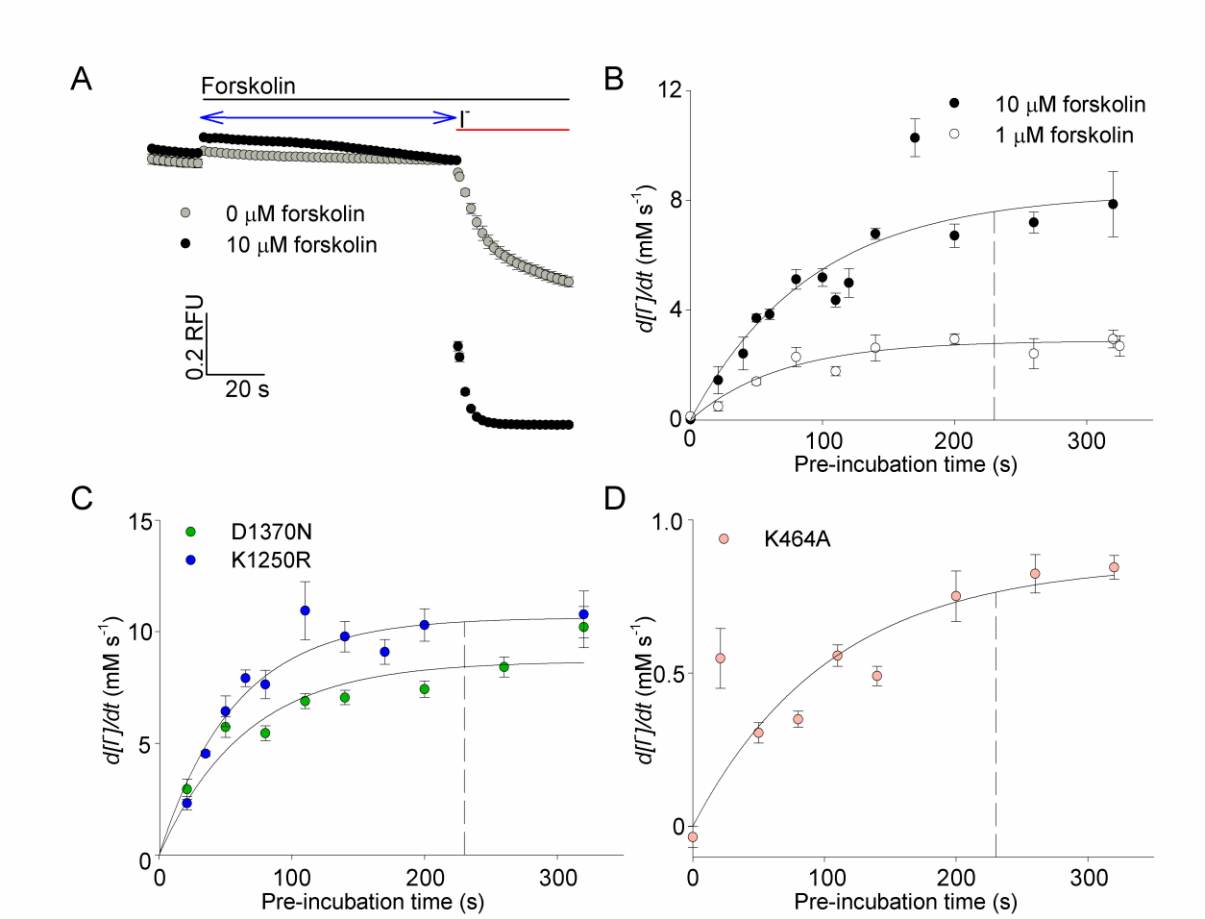
A
Forskolin
I⁻
0 μM forskolin
10 μM forskolin
0.2 RFU
20 s
B
10 μM forskolin
1 μM forskolin
d[I⁻]/dt (mM s⁻¹)
Pre-incubation time (s)
C
D1370N
K1250R
d[I⁻]/dt (mM s⁻¹)
Pre-incubation time (s)
D
K464A
d[I⁻]/dt (mM s⁻¹)
Pre-incubation time (s)

Figure 4

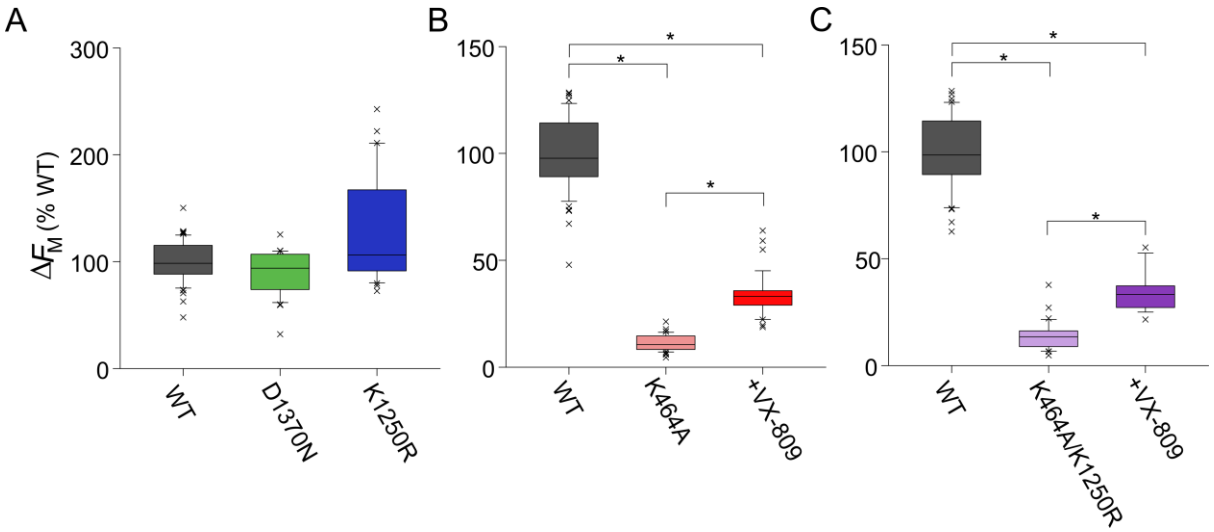
A
B
C
300
200
100
0
ΔF_M (% WT)
WT
D1370N
K1250R
150
100
50
0
*
WT
K464A
+VX-809
WT
K464A/K1250R
+VX-809

Figure 5

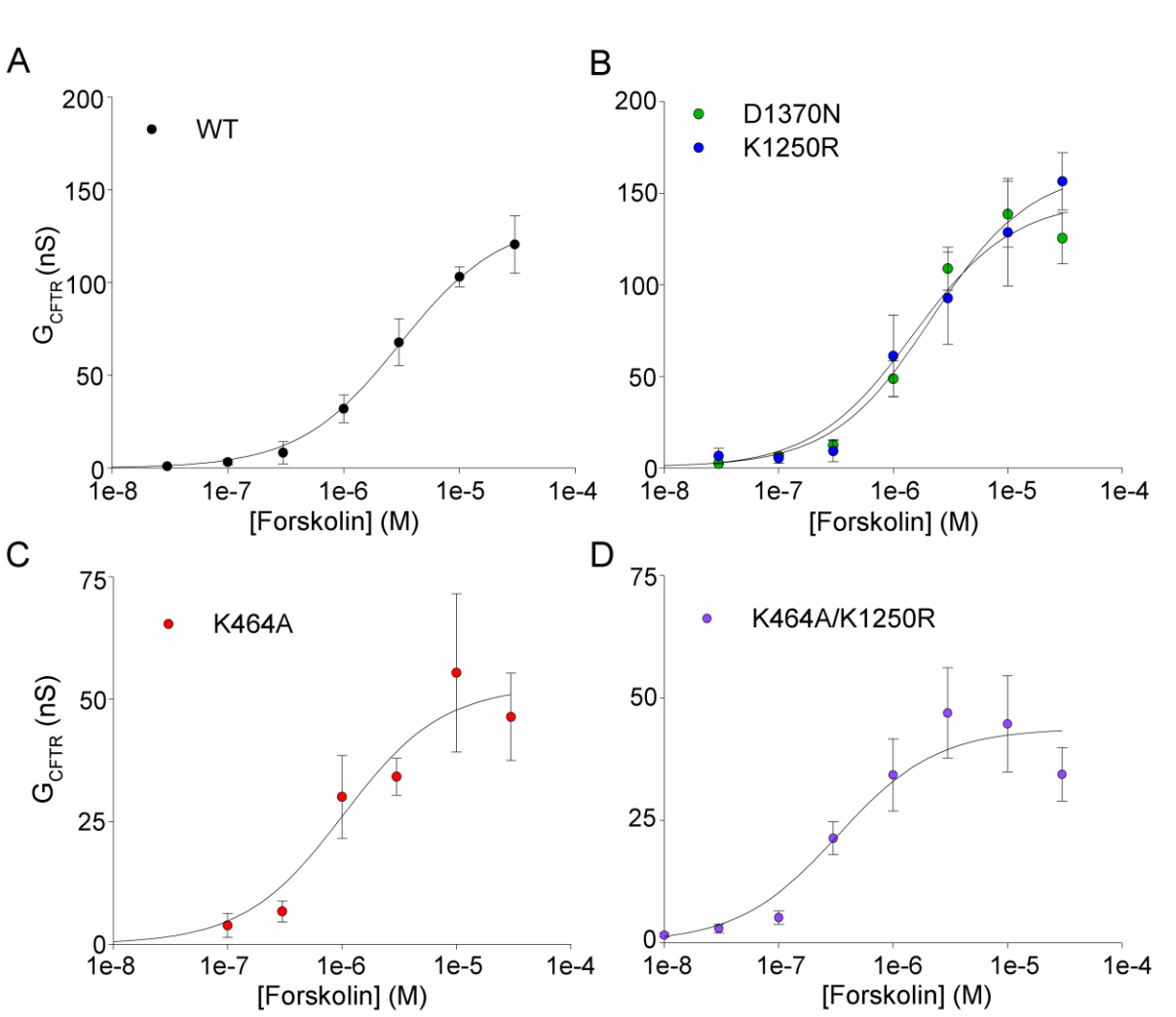
A
WT
B
D1370N
K1250R
C
K464A
D
K464A/K1250R
G_{CFTR} (nS)
[Forskolin] (M)
1e-8
1e-7
1e-6
1e-5
1e-4
0
50
100
150
200
25
75

Figure 6

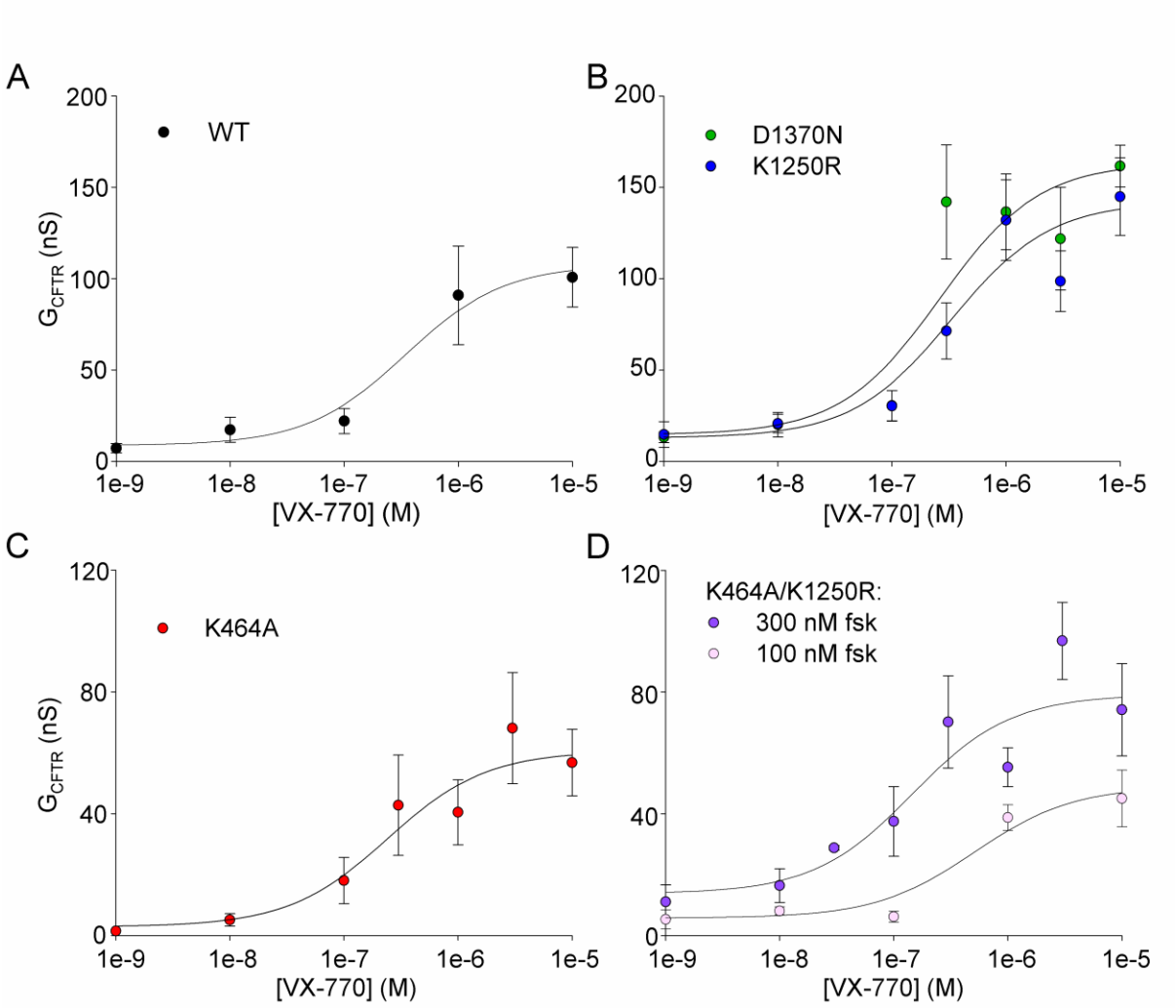
A
WT
G_{CFTR} (nS)
[VX-770] (M)
B
D1370N
K1250R
[VX-770] (M)
C
K464A
G_{CFTR} (nS)
[VX-770] (M)
D
K464A/K1250R:
300 nM fsk
100 nM fsk
[VX-770] (M)

Figure 7

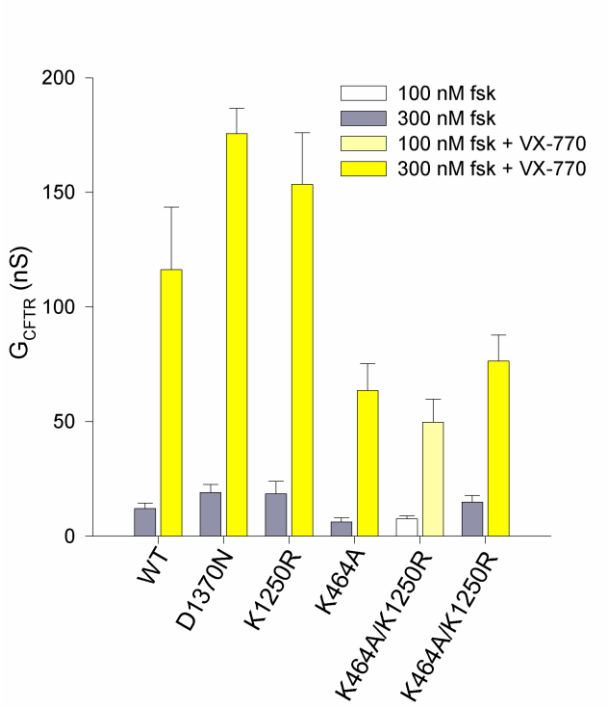
200
150
100
50
0
G_{CFTR} (nS)
100 nM fsk
300 nM fsk
100 nM fsk + VX-770
300 nM fsk + VX-770
WT
D1370N
K1250R
K464A
K464A/K1250R
K464A/K1250R

Figure legends

Figure 1. CFTR gating mechanism. The channel enters a stable open state (O_1) following formation of a head-to-tail NBD dimer, with ATP bound at the two ATP-binding sites formed at the interface. Upon hydrolysis of the ATP bound at site 2 (lower site), the channel closes, via a short-lived post-hydrolytic (O_2) state. >95% of WT-CFTR opening events terminate via hydrolysis of ATP. ~100% of D1370N-CFTR and K1250R-CFTR and ~80% of K464A-CFTR opening events terminate via non-hydrolytic closing. NBD1 = blue, NBD2 = green, TMDs = grey, ATP = yellow, ADP+P_i = orange.

Figure 2. WT-CFTR quenching curves fitted using mathematical model to obtain estimates of CFTR conductance and V_M. Experimental data is shown as normalized fluorescence values (yellow circles). Black lines show time course of anion occupancy of the YFP chromophore predicted by the model: proportion of I^--bound YFP (dotted line, p_{RI}), proportion of Cl^--bound YFP (dashed line, p_{RCl}), and proportion of unoccupied YFP (i.e. fluorescent YFP, solid line, $p_R/p_{R(t0)}$). The latter proportion, like fluorescence, is normalized to the time point immediately preceding I^- addition. (A) 100 nM forskolin quenching curve, and (B) 10 μM forskolin quenching curve. Left panels: fitted using method (1), in which G_{trans} and τ_{trans} are free parameters. Right panels: fitted using method (2), in which G_{trans} and τ_{trans} are constrained to the mean values obtained when CFTR is not activated (13.2 nS and 4.9 s, respectively).

Figure 3. YFP-CFTR protocol optimisation for steady state measurements. (A) WT-CFTR fluorescence time course during incubation with 0 μM or 10 μM forskolin (black bar) and 100 mM extracellular I^- (red bar). The length of pre-incubation (blue arrow) was altered to investigate activation time course in HEK293 cells. (B) Rate of I^- entry following incubation with 1 μM or 10 μM forskolin as a function of pre-incubation time, for WT-CFTR. 1 μM τ = 68.5 s ± 15 s, 10 μM τ = 91.7 s ± 15 s, n = 2 – 10, from 3 plates (for n values corresponding to each individual point see supplementary table SI6). Dashed line indicates time chosen for subsequent experiments, 230 s, beyond which CFTR activation has reached a steady-state. (C) Rate of I^- entry following pre-incubation with 10 μM forskolin, for non-hydrolytic mutants of YFP-CFTR. D1370N-CFTR τ = 64.9 s ± 9 s, K1250R-CFTR τ = 57.1 s ± 8 s, n = 2 – 6, from 2 plates (see SI6). (D) Rate of I^- entry following pre-incubation with 10 μM forskolin for K464A-CFTR, τ = 105.1 s ± 27 s, n = 3 – 6, from 2 plates (see SI6).

Figure 4. Membrane exposure, expressed as a percent of WT-CFTR. (A) WT-CFTR (n = 59, from 11 plates), D1370N-CFTR (n = 32 from 6 plates) and K1250R-CFTR (n = 30 from 6 plates). (B) WT-CFTR (n = 59 from 12 plates) and K464A-CFTR ± 24 h 10 μM VX-809 (n = 42 from 8 plates in absence of VX-809, and n = 35 from 7 plates in presence of VX-809). (C) WT-CFTR (n = 41 from 8 plates) and K464A/K1250R-CFTR ± 24 h 10 μM VX-809 (n = 33 from 6 plates in absence of VX-809, and n = 18 from 4 plates in presence of VX-809). * P < 0.05.

Figure 5. Forskolin concentration-response curves. CFTR conductance estimated using model. (A) WT-CFTR: EC_{50} = 3 μM ± 1.2 μM. (B) D1370N-CFTR: EC_{50} = 1.5 μM ± 0.6 μM.

K1250R-CFTR: EC_{50} = 2.2 µM ± 1.3 µM. (C) VX-809-corrected K464A-CFTR: EC_{50} = 1 µM ± 0.8 µM. (D) VX-809-corrected K464A/K1250R-CFTR: EC_{50} 0.33 µM ± 0.2 µM. Each concentration-response curve is constructed from 4 experiments. For the n value of each concentration-point measurement, see supplementary table SI6.

Figure 6. VX-770 concentration-response curves. CFTR conductance estimated using model. All in the presence of 300 nM forskolin, except (D). (A) WT-CFTR: EC_{50} = 343 nM ± 276 nM. (B) D1370N-CFTR: EC_{50} = 263 nM ± 128 nM. K1250R-CFTR: EC_{50} = 330 nM ± 181 nM. (C) VX-809-corrected K464A-CFTR: EC_{50} = 241 nM ± 179 nM. (D) VX-809-corrected K464A/K1250R-CFTR in the presence of 300 nM forskolin: EC_{50} 145 nM ± 94 nM, or 100 nM forskolin: EC_{50} 510 nM ± 329 nM. Each concentration-response curve is constructed from 6 experiments (or 5 in the case of WT-CFTR and D1370N-CFTR). For the n value of each concentration, see supplementary table SI6.

Figure 7. Summary of potentiation by VX-770. All constructs were potentiated by VX-770 in the presence of 300 nM forskolin. K464A/K1250R-CFTR was tested in both 100 nM and 300 nM forskolin. Bars represent mean estimated CFTR conductance in the presence or absence of saturating VX-770. n = 10 for forskolin in the absence of VX-770 (n = 8 for WT-CFTR and n = 9 for D1370N-CFTR), and n = 6 for forskolin in the presence of VX-770 (n = 4 for WT-CFTR and n = 5 for D1370N-CFTR).

Supplementary Information

SI1. Simple mathematical model allows estimation of G_{CFTR} and V_M parameters from quenching curves.

Cells were modelled as 10 µm-radius spheres and the variables simulated were: intracellular Cl^-, I^- and K^+ concentrations ($[Cl^-]_{in}$, $[I^-]_{in}$ and $[K^+]_{in}$, respectively), membrane potential (V_M) and the proportions of free (p_R) and anion-bound YFP receptor (p_{RI}, p_{RCl}). At the time of I^- addition, CFTR activation has reached a steady-state, and $[Cl^-]_{in}$, $[I^-]_{in}$ and $[K^+]_{in}$ are assumed to have equilibrated with the extracellular concentrations of these ions. Equilibrium potentials (E_{Cl}, E_I and E_K) were calculated from the Nernst Equation: for a generic anion *i*, at 37 °C

$$E_i = -62 \text{ mV } \text{Log}_{10} \frac{[i]_{out}}{[i]_{in}}$$

Whole-cell ionic currents (I_i) were calculated as

$$I_i = \frac{G_{MAXi}\, V_m}{140\ mM} * \frac{[i]_{in} - [i]_{out}\, e^{-zF/RT}}{1 - e^{-zF/RT}}$$

Where G_{MAX} is the maximal whole-cell conductance expected in symmetrical 140 mM solutions of ion *i*, z is the ion valence, *F*, *R* and *T* have their usual thermodynamic meanings. Currents for I^-, Cl^- (carried by CFTR) and an endogenous leak K^+ conductance of 2.5 nS (Rapedius et al., 2005) were simulated. In addition, it was necessary to include a transient anion conductance, G_{trans}, with a single exponential decay characterized by time constant τ_{trans}. As mentioned in Methods, this is likely an endogenous conductance of the HEK293 cells, unrelated to CFTR.

At each time point, ionic currents, molar fluxes and corresponding changes in intracellular concentration of ions were calculated. The change in membrane potential due to the net ionic current was obtained using an estimated membrane capacitance (C_M) of 1 µF/cm^2 (including a 50% increase in surface area due to plasma membrane invaginations, Gentet et al., 2000)

$$\frac{dV_M}{dt} = -\frac{I_I + I_{Cl} + I_K + I_{trans}}{C_M}$$

The anion binding site on the YFP chromophore, can be unoccupied or occupied by I^- or Cl^-. Intracellular ionic concentrations were used to calculate, at each time point, the proportion of YFP chromophores with bound anion. For instance, the proportion of I^--bound receptors, p_{RI}, was calculated as

$$p_{RI} = \frac{[I\text{-}]_{in}}{[I\text{-}]_{in} + K_I\left(1 + \frac{[Cl\text{-}]_{in}}{K_{Cl}}\right)}$$

While the proportion of YFP with an unoccupied anion-binding site is given by

$$p_R = \frac{1}{1 + \frac{[Cl\text{-}]_{in}}{K_{Cl}} + \frac{[I\text{-}]_{in}}{K_I}}$$

To simulate fluorescence values normalized to the time of I^- addition, the value of p_R was divided by the value of p_R calculated for the starting time point. The parameter values optimized by fitting the time course of $p_R/p_{R(t0)}$ to F/F_{max} were

G_{CFTR}: steady-state CFTR conductance
V_M: membrane potential at time of I^- addition
G_{trans}: transient endogenous anion conductance
τ_{trans}: exponential decay time constant for transient endogenous anion conductance
In some cases, as described in Methods, the values for the transient endogenous anion conductance were constrained to those estimated in control conditions. Regression was performed by minimizing the sum of squared residuals, using the Nelder-Mead simplex algorithm in the MATLAB environment. Files are available, upon request.

SI2. Transient anion conductance is not CFTR-dependent

Comparison of basal YFP quenching (without any forskolin or vehicle pre-treatment) in cells expressing either WT-CFTR or G551D-CFTR. The G551D mutation reduces P_o to negligible values (Bompadre et al., 2007), but is known not to affect processing. Thus the two YFP-CFTR variants have comparable cellular distribution, but any CFTR-dependent anion conductance is ablated by the mutation. Estimated conductances, and the traces shown (circles show measured data, solid lines use these parameters: WT G_{CFTR} = 1.4 nS, V_M = --82 mV, G_{trans} = 10.5 nS and τ_{trans} = 4.0 s. G551D G_{CFTR} = 0.1 nS, V_M = -83 mV, G_{trans} = 10.4 nS and τ_{trans} = 6.1 s), are consistent with cells expressing G551D-CFTR being transiently permeant to anions, with the amplitude of this conductance decreasing to zero within the first 10-20 s, following which no further quenching is observed. In the cells expressing WT-CFTR cultured in parallel, by contrast, while quenching is initially very similar to that seen in the cells expressing mutant channels, a slow (note amplified y-axis scale) further quenching persists throughout the 40 s, reflecting the continued presence of a driving force for I^- entry, and a small anion conductance likely reflecting the low levels of phosphorylated CFTR present in basal conditions.

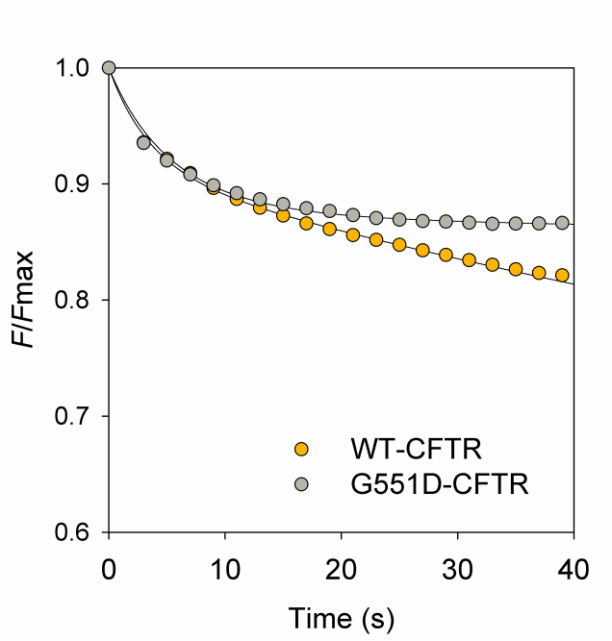

SI3. Non-stationary assay. The time course of activation by forskolin was not significantly altered by the mutations studied in this paper (Fig. 3). 230 s was identified as a time at which CFTR was gating close to steady-state for all mutants studied. Interestingly, lowering the concentration of forskolin did not increase the time constant, suggesting a high rate of dephosphorylation dominating the macroscopic observed rate at which CFTR activates (see Table).

[Fsk] μM	**τ (s)**	**± (s)**
30	48.6	12
10	91.7	15
3	106.2	24
1	68.5	15

SI4. Forskolin concentration-response curves, quantified with V_M estimated using model. (A) WT-CFTR: EC_{50} = 825 nM ± 1.2 µM. (B) D1370N-CFTR: EC_{50} = 113 nM ± 62 nM. K1250R-CFTR: EC_{50} = 139 nM ± 139 nM. (C) VX-809-corrected K464A-CFTR: EC_{50} = 988 nM ± 876 nM. (D) VX-809-corrected K464A/K1250R-CFTR: EC_{50} 168 nM ± 127 nM. n = 4.

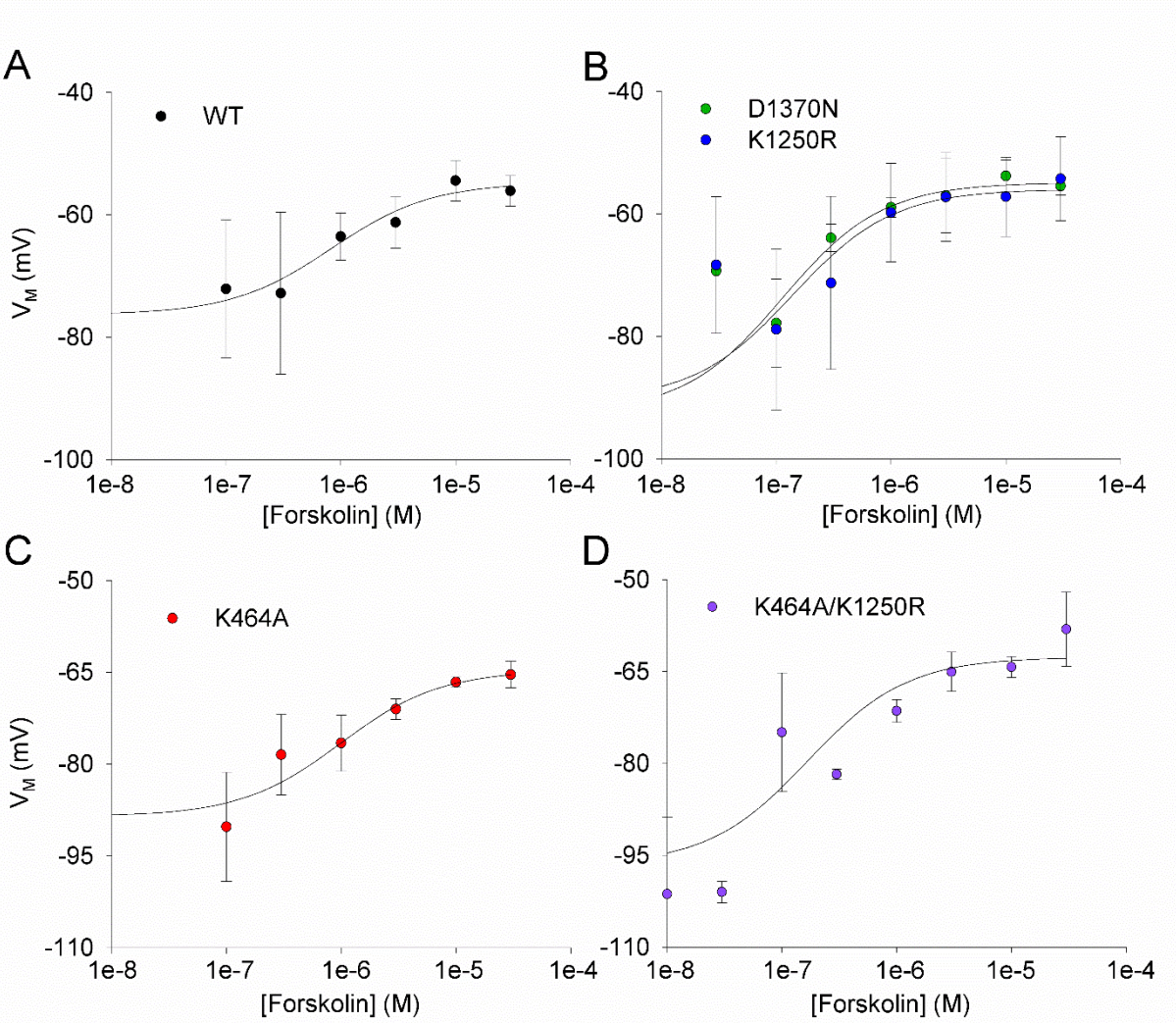

SI5. VX-770 concentration-response curves, quantified with V_M estimated using model. (A)-(C) all in the presence of 300 nM forskolin. (A) WT-CFTR: EC_{50} = 116 nM ± 144 nM, n = 5. (B) D1370N-CFTR: EC_{50} = 11 nM ± 16 nM, n = 5. K1250R-CFTR: EC_{50} = 4.3 nM ± 5 nM. (C) VX-809-corrected K464A-CFTR: EC_{50} = 87 nM ± 107 nM. (D) VX-809-corrected K464A/K1250R-CFTR in the presence of 300 nM forskolin: EC_{50} 52 nM ± 42 nM, or 100 nM forskolin: EC_{50} 121 nM ± 177 nM. Unless otherwise stated, n = 6.

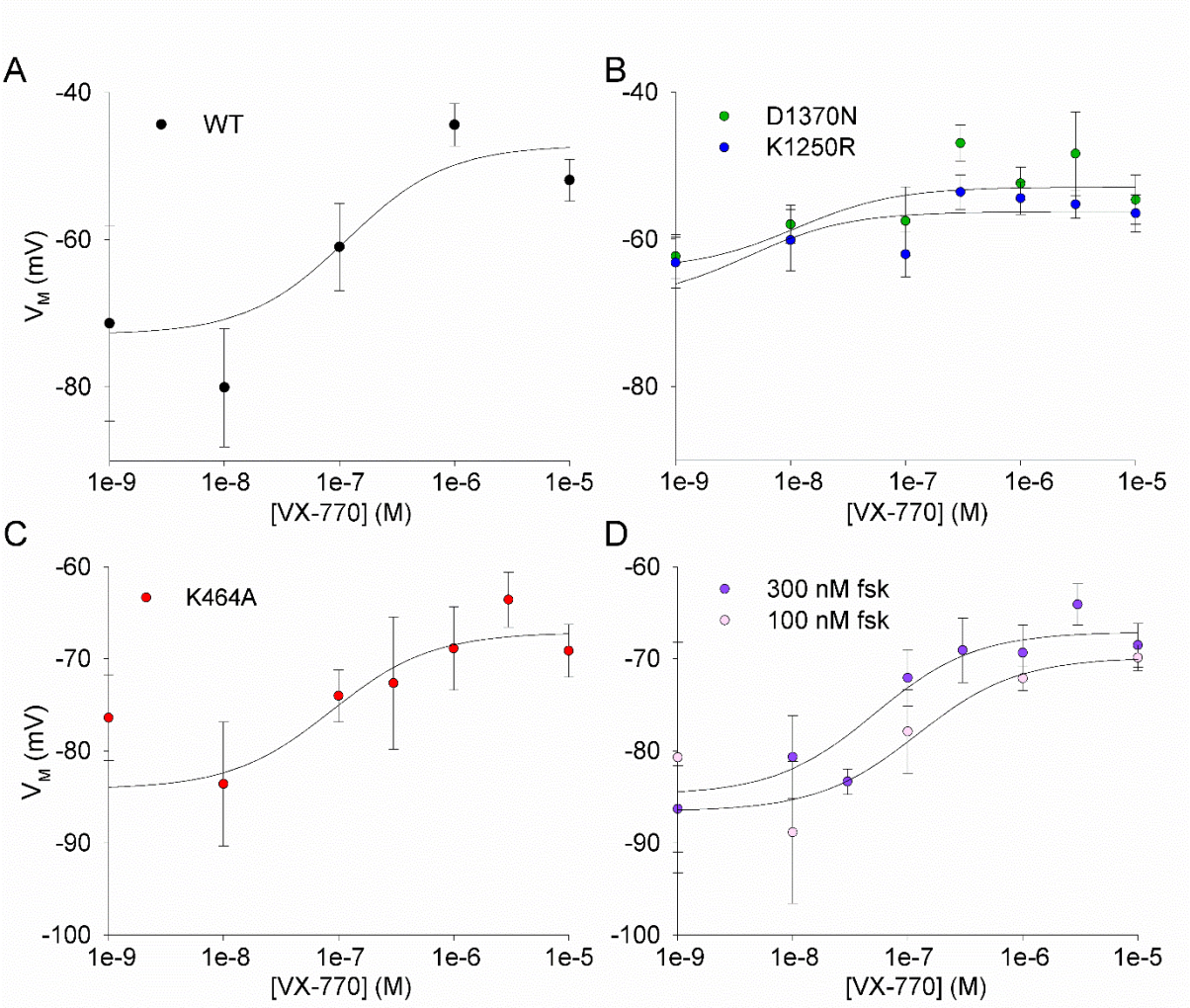

SI6. n values for individual points on time course activation curves and concentration-response curves

Figure 3B

10 µM fsk

Time (s)	n	Plates
0	3	1
21	8	3
40	3	1
50	3	1
60	3	1
80	9	3
100	3	1
110	2	1
120	3	1
140	5	2
170	3	1
200	6	2
260	3	1
320	4	2

1 µM fsk

Time (s)	n	Plates
0	6	2
21	9	3
50	6	2
80	8	3
110	2	1
140	3	2
200	10	3
260	6	2
320	6	3
325	2	2

Figure 3C

D1370N

Time (s)	n	Plates
0	3	1
21	6	2
50	6	2
80	5	2
110	5	2
140	6	2
200	6	2
260	6	2
320	5	2

Figure 3C

K1250R

Time (s)	n	Plates
0	6	2
21	5	2
35	4	2
50	5	2
65	2	1
80	4	2
110	4	2
140	5	2
170	6	2
200	5	2
320	4	2

Figure 3D

K464A

Time (s)	n	Plates
0	3	1
21	6	2
50	6	2
80	5	2
110	6	2
140	5	2
200	6	2
260	6	2
320	6	2

Figure 5A

WT

[Fsk] (M)	n
0	3
3.00E-08	1
1.00E-07	4
3.00E-07	2
1.00E-06	4
3.00E-06	4
1.00E-05	4
3.00E-05	4

Figure 5B

D1370N

[Fsk] (M)	n
0	4
3.00E-08	1
1.00E-07	4
3.00E-07	2
1.00E-06	4
3.00E-06	4
1.00E-05	4
3.00E-05	4

K1250R

[Fsk] (M)	n
0	4
3.00E-08	2
1.00E-07	3
3.00E-07	3
1.00E-06	4
3.00E-06	4
1.00E-05	4
3.00E-05	4

Figure 5C
K464A

[Fsk] (M)	n
0	3
1.00E-07	4
3.00E-07	2
1.00E-06	4
3.00E-06	4
1.00E-05	4
3.00E-05	4

Figure 5D
K464A/K1250R

[Fsk] (M)	n
0	4
1.00E-08	2
3.00E-08	2
1.00E-07	4
3.00E-07	2
1.00E-06	4
3.00E-06	4
1.00E-05	4
3.00E-05	4

Figure 6A
WT

[VX-770] (M)	n
0	6
1.00E-09	4
1.00E-08	4
1.00E-07	5
1.00E-06	5
1.00E-05	6

Figure 6B
D1370N

[VX-770] (M)	n
0	8
1.00E-09	4
1.00E-08	5
1.00E-07	5
3.00E-07	2
1.00E-06	8
3.00E-06	2
1.00E-05	7

K1250R

[VX-770] (M)	n
0	7
1.00E-09	3
1.00E-08	6
1.00E-07	6
3.00E-07	5
1.00E-06	7
3.00E-06	5
1.00E-05	7

Figure 6C
K464A

[VX-770] (M)	n
0	5
1.00E-09	2
1.00E-08	6
1.00E-07	6
3.00E-07	4
1.00E-06	6
3.00E-06	4
1.00E-05	6

Figure 6D
K464A/K1250R

[VX-770] (M)	n
0	6
1.00E-09	4
1.00E-08	6
3.00E-08	2
1.00E-07	6
3.00E-07	4
1.00E-06	6
3.00E-06	4
1.00E-05	6

References

Bompadre, S.G., Sohma, Y., Li, M., and Hwang, T.-C. (2007). G551D and G1349D, Two CF-associated Mutations in the Signature Sequences of CFTR, Exhibit Distinct Gating Defects. J. Gen. Physiol. *129*: 285-98.

Gentet, L.J., Stuart, G.J., and Clements, J.D. (2000). Direct Measurement of Specific Membrane Capacitance in Neurons. Biophys. J. *79*: 314–320.

Rapedius, M., Soom, M., Shumilina, E., Schulze, D., Schönherr, R., Kirsch, C., et al. (2005). Long chain CoA esters as competitive antagonists of phosphatidylinositol 4,5-bisphosphate activation in Kir channels. J. Biol. Chem. *280*: 30760–30767.